

Controlled release of multiphoton quantum states from a microwave cavity memory

Wolfgang Pfaff^{1,2*}, Christopher J. Axline^{1,2}, Luke D. Burkhardt^{1,2}, Uri Vool^{1,2}, Philip Reinhold^{1,2}, Luigi Frunzio^{1,2}, Liang Jiang^{1,2}, Michel H. Devoret^{1,2} and Robert J. Schoelkopf^{1,2}

Signal transmission loss in a quantum network can be overcome by encoding quantum states in complex multiphoton fields. But transmitting quantum information encoded in this way requires that locally stored states can be converted to propagating fields. Here we experimentally show the controlled conversion of multiphoton quantum states, such as Schrödinger cat states, from a microwave cavity quantum memory into propagating modes. By parametric conversion using the nonlinearity of a single Josephson junction, we can release the cavity state in ~ 500 ns, about three orders of magnitude faster than its intrinsic lifetime. This mechanism—which we dub Schrödinger’s catapult—faithfully converts arbitrary cavity fields to travelling signals with an estimated efficiency of $> 90\%$, enabling the on-demand generation of complex itinerant quantum states. Importantly, the release process can be precisely controlled on fast timescales, allowing us to generate entanglement between the cavity and the travelling mode by partial conversion.

A powerful way to tame complexity when scaling up a quantum system is to construct it as a network. Breaking up the whole into small, testable modules that are connected through well-defined communication channels reduces undesired crosstalk and minimizes the spreading of errors through the system. Therefore, quantum networks have been proposed for quantum information processing (QIP)¹ and it has been shown theoretically that there are favourable thresholds for quantum error correction for such modular architectures, even with noisy quantum communication channels². Experiments with multiple platforms are underway at present to realize prototypes of quantum networks^{3–5}. The key requirement hereby is the ability to interface quantum states stored and processed in network nodes with propagating states that connect the nodes.

Quantum continuous variables (CV) allow versatile and robust encoding of quantum information in higher-dimensional Hilbert spaces. For instance, encoding quantum bits in CV systems can provide the redundancy required to enable quantum error correction⁶. Non-Gaussian CV states that could be used as QIP-enabling resources have been created experimentally in the states of ion motion⁷ and atomic spins^{8,9}, as well as optical^{10,11} and microwave photons^{12–15}. In particular, microwave cavities in superconducting circuits have recently further enabled the storage¹⁶ and protection¹⁷ of quantum information encoded in non-Gaussian oscillator states. Using these locally stored states as resources in an error-protected, network-based QIP architecture hinges on the ability to interface them with travelling signals (Fig. 1a). However, the controlled mapping of general multiphoton states between a CV quantum memory and travelling signals has so far remained an outstanding challenge.

Here, we experimentally demonstrate the controlled conversion of non-classical multiphoton states from a superconducting microwave cavity to propagating states. Using radiofrequency-controlled four-wave mixing in a single Josephson junction we are able to evacuate the cavity about three orders of magnitude faster than its natural lifetime. The field is coherently and efficiently

upconverted in frequency, and released into a transmission line. This enables on-demand generation of travelling multiphoton quantum states of high fidelity. The excellent temporal control over the conversion process allows shaping of the emitted wave packet. We use this capability to release only a part of the state stored in the cavity; this partial conversion creates entanglement between the stationary and travelling fields in multiple encodings, confirmed by the observation of non-classical correlations.

Coupling stationary to propagating microwaves

To enable communication between network nodes with multiphoton states, a coherent release must meet several important criteria. First, in order to enable distribution of quantum information with high fidelity we require a large ‘on/off ratio’. In the ‘off’-state the coherence of the memory must be preserved, whereas the ‘on’-state allows fast, on-demand release. Further, successful communication requires faithful state mapping, independent of the number of photons. Thus, each photon in the memory should be removed, described by the annihilation operator \hat{a} , while creating an outgoing photon, described by the creation operator \hat{b}^\dagger . This conversion interaction is effectively a ‘beam splitter’, with Hamiltonian $H_{\text{conv}} \propto \hat{a}\hat{b}^\dagger + \text{h.c.}$ Finally, shaping the wave packet is required to enable capture by a receiving node¹⁸ and to generate entanglement; we therefore demand precise temporal control over the release process.

Several approaches have been used to map stationary onto travelling states in superconducting quantum circuits. Tuning the coupling between a superconducting artificial atom and an output mode allows the generation and shaping of single photons^{19–22}. However, no interface between locally stored and travelling arbitrary CV quantum states has been demonstrated so far. Quasi-classical oscillator states have been successfully mapped using dedicated coupling elements such as flux-tunable couplers^{23,24} or parametric converters²⁵, which require tuning by external magnetic flux. To date, integration of flux-tuning methods with the kind of high-Q

¹Departments of Applied Physics and Physics, Yale University, New Haven, Connecticut 06520, USA. ²Yale Quantum Institute, Yale University, New Haven, Connecticut 06520, USA. *e-mail: wolfgang.pfaff@yale.edu

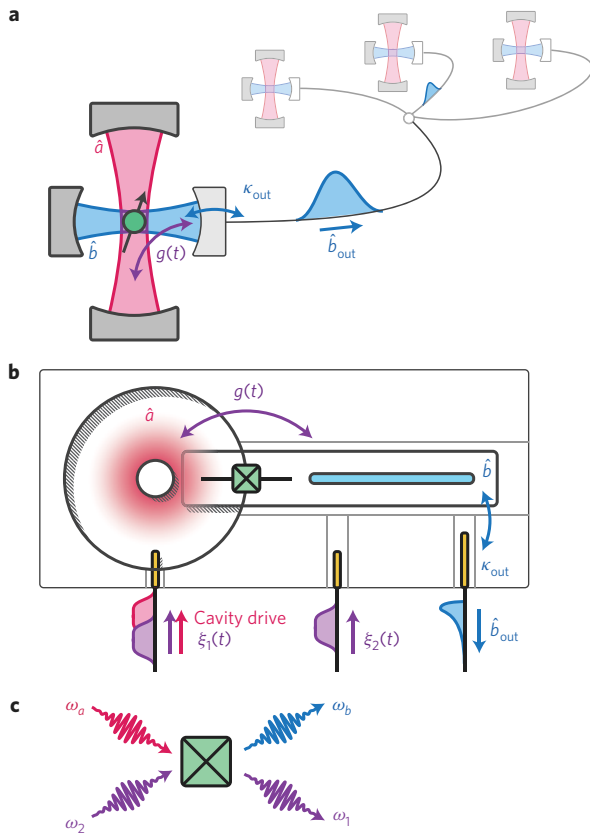


Figure 1 | Nodes in a quantum network using high-Q cavities as memories.

a, We envisage an architecture in which each node consists of a high-Q storage mode (described by \hat{a}), an output mode (\hat{b}) coupled to a transmission channel (\hat{b}_{out}) with a rate κ_{out} , and a nonlinear system—such as an atom (green)—that allows for a tunable coupling $g(t)$ between a and b . This coupling allows transfer between a and b_{out} , and thus transfer of states between nodes. **b**, Three-dimensional circuit QED implementation of a single node (schematic top view). The storage mode is the fundamental mode of a coaxial cavity (here, $\omega_a/2\pi = 4.1$ GHz). The output resonator is a $\lambda/2$ stripline resonator (here, $\omega_b/2\pi = 10.0$ GHz), fabricated on the same chip as a single-junction transmon (green) that couples capacitively to both modes. The chip is inserted through a waveguide tunnel. Strongly undercoupled input pins (left and middle) allow application of radiofrequency tones (envelopes shown schematically), and signals leave b to a transmission line through an output coupler pin (here, $\kappa_{\text{out}}/2\pi = 640$ kHz). Qubit control and measurement tones are applied through the input port of the output resonator (Supplementary Information). **c**, Coupling between the resonator modes is realized by tunable pump tones $\xi_{1,2}(t)$ that enable four-wave mixing through the transmon junction. Annihilation and creation of pump photons with frequencies $\omega_{1,2}$ result in upconversion from a to b if $|\omega_1 - \omega_2| = |\omega_a - \omega_b|$.

storage cavities we intend to use for synthesizing, storing, and protecting complex quantum states remains an open challenge.

Our strategy for realizing an interface between arbitrary stationary and travelling multiphoton quantum states is sketched in Fig. 1a. We aim to couple a storage cavity mode, a , and an output mode, b , by a nonlinear element that enables photon conversion between them. Instead of using a dedicated flux-tunable converter element, we choose to couple the modes using only a fixed-frequency transmon artificial atom in the strongly dispersive regime of cavity quantum electrodynamics (QED)²⁶. The single Josephson junction of the transmon provides the required nonlinearity, while preserving cavity coherence on the order of milliseconds¹⁶. Our experimental scheme is shown in Fig. 1b. A high-Q superconducting

cavity and a low-Q output resonator that are strongly detuned ($|\omega_a - \omega_b|/2\pi \approx 6$ GHz) are both coupled to the transmon. The output mode is further coupled with rate $\kappa_{\text{out}} = 1/250$ ns to a transmission line mode, b_{out} , where the emitted signals are amplified and recorded (Supplementary Information). This configuration enables a long memory life time, $\kappa_0 = 1/450$ μ s, while still allowing for fast readout and control of arbitrary quantum states²⁷.

Crucially, the nonlinearity induced by the transmon allows conversion of multiphoton states between the memory and output with a large on/off ratio. The Hamiltonian describing the coupling between the modes is given by (see ref. 28)

$$H/\hbar = -E_J \cos(\phi_a(\hat{a} + \hat{a}^\dagger) + \phi_b(\hat{b} + \hat{b}^\dagger) + \phi_c(\hat{c} + \hat{c}^\dagger)) \quad (1)$$

where \hat{c} is the annihilation operator for the transmon mode, E_J is the Josephson energy, and ϕ_i is the zero-point fluctuation of flux associated with the respective mode. Because the cosine-coupling enables all four-wave mixing processes that conserve energy, we can create interactions between the strongly detuned resonator modes by applying pump tones. In particular, two pumps with a frequency difference matching the detuning of the resonators enable the conversion Hamiltonian

$$H_{\text{conv}}/\hbar = g(t)\hat{a}\hat{b}^\dagger + g^*(t)\hat{a}^\dagger\hat{b} \quad (2)$$

where the coupling $g(t) = E_J\phi_a^2\phi_b^2\xi_1^*(t)\xi_2(t)$ can be controlled by the pump strengths $\xi_{1,2}(t)$ (Fig. 1c). Note that the dressed transmon mode c does not directly participate in this conversion. From the output mode, photons converted from a to b leak into the transmission line. For $g \ll \kappa_{\text{out}}$, this results in an effective damping of a with rate $\kappa = 4g^2/\kappa_{\text{out}}$; the fastest achievable damping is given by the bandwidth of the output mode, κ_{out} , corresponding to a maximum on/off ratio of the decay that exceeds 10^3 (Supplementary Information).

Cavity evacuation

We first explore the maximum damping rate we can induce with pump tones of varying strength (Fig. 2a). We prepare the Fock state $|1\rangle$ in the cavity, and then monitor the cavity population over time while applying the pumps with frequencies ω_1 and ω_2 . The pump frequencies are tuned on resonance with the conversion process of equation (2) using $\omega_a - \omega_1 = \omega_b - \omega_2 = 2\pi \times (30\text{--}50)$ MHz. Increasing the pump strength allows us to tune the cavity energy decay rate from its intrinsic value of $\kappa_0 = 1/0.45$ ms to $\kappa \approx 1/0.5$ μ s for $g/2\pi = 207$ kHz, the maximum conversion rate achievable with the available pump power (Fig. 2b). At this point, $g \approx 0.3 \times \kappa_{\text{out}}$, and the decay becomes limited by the bandwidth of the output mode. We can thus use this ‘Q-switch’ to evacuate the storage mode with an on/off ratio approaching 10^3 .

This Q-switch is very close to an ideal damping of the memory. It cools the cavity close to the vacuum, with a residual population of $\bar{n} \lesssim 0.01$, the noise floor of our measurement. We can therefore use the conversion as a fast reset, which is a useful tool for experiments with long-lived quantum memories^{27,29}. Further, the measured decay of the cavity population is in excellent agreement with predictions based on theory and independent calibrations of the pump strengths. This agreement, together with the absence of any significant heating in the system, suggests a very high conversion efficiency from the storage to the output mode. We estimate that the loss rate into undesired channels, κ_{loss} , is about 0.01κ , corresponding to an expected inefficiency of the conversion of $1 - \eta_{\text{conv}} \approx 0.01$ (Supplementary Information).

We verify that the cavity evacuation is independent of the input state. We prepare larger Fock states and monitor the population of the input Fock state, $P(n)$ (Fig. 2c). For state-independent damping of a harmonic oscillator, with only a single-photon decay operator

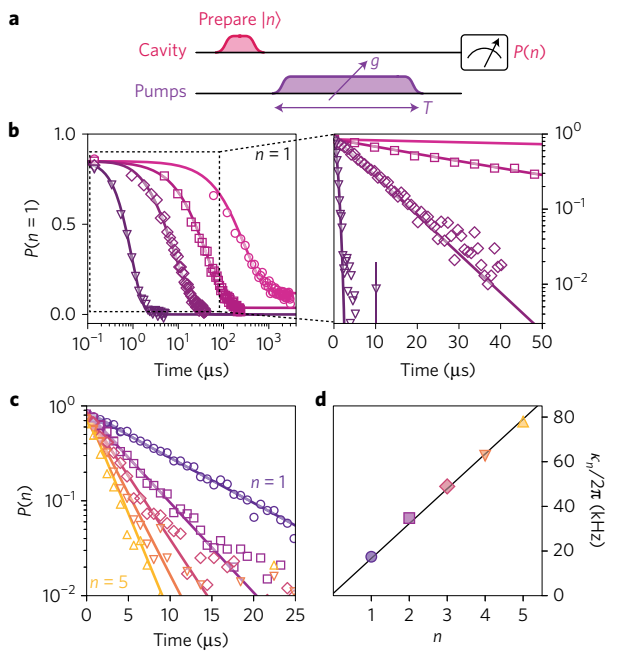


Figure 2 | Cavity damping by mode-conversion. **a**, Measurement scheme. After preparing the cavity in a Fock state, we monitor the population as a function of time for different pump strengths. The pump tones have constant amplitude in time, up to a smooth ring-up and ring-down. **b**, Decay of the single-photon state $|1\rangle$. $g/2\pi = 0$ (circles), 25 kHz (squares), 54 kHz (diamonds), and 207 kHz (triangles). Solid lines: for $g = 0$, exponential fit, yielding the natural decay time; for $g > 0$, theoretical prediction based on independently calibrated pump parameters. For large g the decay is not simply described by a single exponential (Supplementary Information). The last datapoint for the fastest decay shows the average and standard deviation for the residual cavity population, consistent with the vacuum state ($P(1) = 0.01 \pm 0.01$). For small or vanishing g ($\lesssim 30$ kHz), the equilibrium state of the cavity is a small thermal state (Supplementary Information). **c**, Decay of number states $|n\rangle$, with n ranging from 1 to 5; $g/2\pi = 54$ kHz. Solid lines are single-exponential fits $P(n) \propto \exp(-\kappa_n t)$. **d**, Extracted decay rates κ_n . Solid line is a linear fit to $\kappa_{\text{loss}} + n\kappa$, where κ_{loss} is the independently measured loss rate (Supplementary Information).

\hat{a} , we expect the state $|n\rangle$ to decay with a rate $\kappa_n = n\kappa$. From exponential fits to the decay of $P(n)$ we find very good agreement with this linear behaviour (Fig. 2d). For larger n we expect that κ_n will gradually decrease due to the Kerr effect¹⁴. For $n \leq 5$ we find a deviation of κ_n from $n\kappa_1$ of $\leq 6\%$, and therefore state independence is a good approximation (Supplementary Information). This can be improved further by reducing the magnitude of the Kerr effect through adjustment of sample parameters.

Travelling multiphoton quantum states

To determine whether cavity states are mapped faithfully onto travelling signals we characterize the field emitted during conversion. We prepare a cavity state and record the field using heterodyne detection with a quantum-limited amplifier³⁰ (Fig. 3a). The averaged in-phase signal, $\langle I(t) \rangle$, from releasing a coherent state with average photon number $\bar{n} = 1$ is shown in Fig. 3b. Because the output mode has a finite bandwidth, we observe an exponential rise of the signal at rate κ_{out} , followed by an exponential decay with the induced decay rate κ . The emitted signal clearly retains coherence with the cavity state, made visible as an oscillation by demodulating with a small detuning from the output frequency. Importantly, the amplitude of the oscillations is consistent with a high conversion efficiency from the cavity to the output mode. By calibrating the signal amplitude in terms of the number of photons emitted by the

output resonator, we estimate that the propagating field contains 1 ± 0.15 photons; this is in agreement with our expectation of a small inefficiency in the conversion (Supplementary Information).

A crucial requirement for our interface is that non-classical states are preserved faithfully in the conversion process. Because the averaged signal vanishes for most states of interest, we compute a probability distribution in phase space. By integrating each measurement record $I(t) + iQ(t)$ in time and histogramming the results, we directly obtain the Husimi Q-function^{20,31}. The measured Q-functions for the vacuum and a coherent state with $\bar{n} = 1$ are shown in Fig. 3c. Finite loss in our detection circuitry leads to a smoothing and shrinking of the distribution, the extent of which is determined by the detection efficiency η_{det} (ref. 31). The coherent state is thus not centred at $|\alpha| = 1$, but is moved closer to the origin. Having established a conversion efficiency of close to unity, the position of the coherent-state population in the Q-function is a direct measure of our detection efficiency; assuming no loss in the conversion we obtain $\eta_{\text{det}} = 0.43 \pm 0.04$, consistent with the expected performance of our amplifier (Supplementary Information). Although non-classical features are thus blurred by the detector, state-essential signatures are preserved in the raw data; knowledge of the detection efficiency allows us to quantitatively confirm the faithful release of quantum states. We illustrate this using two classes of non-Gaussian oscillator states.

The first class are Fock state superpositions of the form $(|0\rangle + |n\rangle)/\sqrt{2}$, which display an n -fold symmetry in their quasiprobability distributions. For a set of such states we show the Wigner function of the cavity state, measured directly after preparation³², and the Q-function of the released field (Fig. 3d); from comparison it is clear that the two distributions share the same symmetry. For additional clarity, we integrate the Q-function radially to obtain a probability distribution as a function of angle, $\text{Pr}(\phi)$. In this representation it can be seen that the symmetry is fully preserved; the contrast is as expected, given our detection efficiency.

A second class of states of particular interest for CV quantum information processing are ‘Schrödinger cat’ states of the form $|\mathcal{C}_\alpha^\pm\rangle = \mathcal{N}(|\alpha\rangle \pm |-\alpha\rangle)$, which are eigenstates of photon number parity. We create and release the even (+) and odd (−) parity coherent-state superpositions $|\mathcal{C}_{\sqrt{2}}^\pm\rangle$ with average photon number $|\alpha|^2 = \bar{n} = 2$ (Fig. 3e). Because in heterodyne detection only the Q-function is directly accessible, the characteristic coherence fringes are strongly suppressed in the travelling field data; as a result, the distributions appear fairly similar. However, subtracting the marginals—obtained by integrating the Q-function along one axis—clearly reveals a difference, with a magnitude that is consistent with our detection efficiency and a high degree of state preservation. The heterodyne detection used in this experiment limits the number of photons accessible to about five; we estimate that in this regime the fidelities with the ideal states exceed 90% (Supplementary Methods).

The release of the cavity states shown can enable error-correctable transmission of quantum information. Because we have temporal control over the pump tones, we can shape the wave packet, which enables capture of emitted fields by a receiving module¹⁸ (Supplementary Information). An inherent challenge for this direct quantum state transmission is that inevitable photon loss in the transmission channel will corrupt the received state. However, by choosing an appropriate encoding, the receiver will be able to detect and correct this error. For example, the states $|2\rangle$ and $(|0\rangle + |4\rangle)/\sqrt{2}$ are codewords of a binomial code³³ that can readily be sent by our system. Single-photon loss in the transmission channel will result in a change of parity, which can be detected and corrected by a receiver.

Entanglement between stationary and travelling fields

We next show that temporal control over the pumps allows us to generate entanglement between cavity and travelling modes by

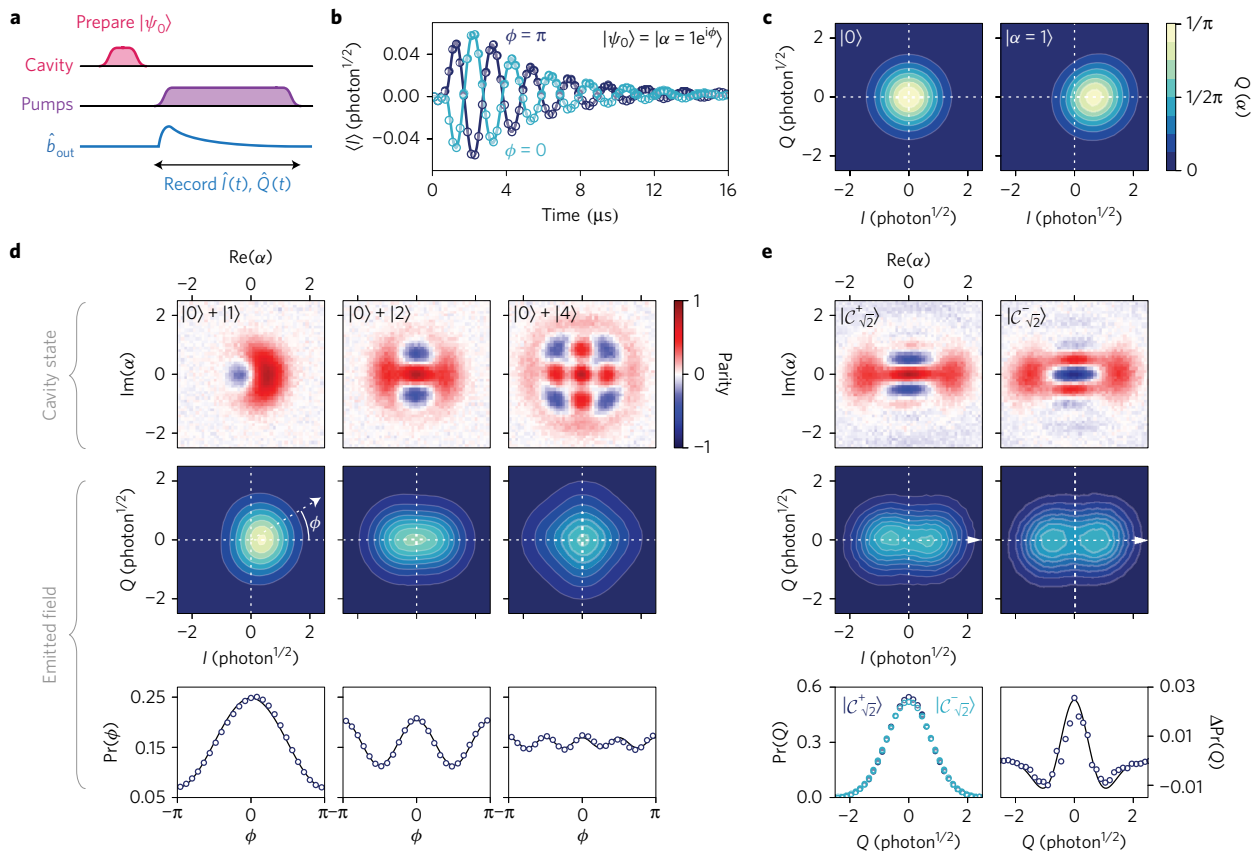


Figure 3 | Travelling multiphoton quantum states. **a**, After preparing a cavity state, we monitor the output field in heterodyne detection while applying the pump tones. **b**, Averaged in-phase signal for two coherent states with $\bar{n}=1$ and opposite phases. $g/2\pi=125$ kHz for this data. Solid lines: fit to a sum of two exponentials with sinusoidal oscillation, $\langle I(t) \rangle \propto (\exp(-\kappa t) - \exp(-\kappa_{out} t)) \times \cos(2\pi f t + \phi_{\pm})$. f is the finite difference between the signal and demodulation frequencies, and ϕ_{\pm} are the phases of the resulting signals, corresponding to prepared states $|\pm\alpha\rangle$; here, $\phi_- = \pi - \phi_+$. **c**, Q-functions for vacuum and a coherent state obtained by integrating quadrature data in time and computing normalized histograms. **d**, Fock state superpositions $(|0\rangle + |n\rangle)/\sqrt{2}$. Top panel: Measured Wigner function of the prepared cavity state (not corrected for imperfect readout). Middle: Q-function of the travelling signal, not corrected for detection loss. Bottom: radially integrated Q-function, $\text{Pr}(\phi) = \int r Q(r, \phi) dr$. Solid line: expected contrast for the ideal state, taking into account the detection efficiency. **e**, Even and odd cat states, $|C_{\sqrt{2}}^{\pm}\rangle$. Lower left: marginals $\text{Pr}(Q)$, obtained by integrating over I (arrows indicate direction of integration). Lower right: Difference between the marginals (odd subtracted from even). Solid lines: expected signals for the ideal states, taking into account the detection efficiency. All Q-function data have been taken with $g/2\pi = 164$ kHz. Fock state superposition Q-functions were taken with 10^7 samples; cat state Q-functions with 10^6 samples.

partial conversion. We use the large on/off ratio over the release process to convert only a part of the energy stored in the cavity; this is the analogue of a partially reflective beam splitter, and can thus generate entanglement between the reflected (remaining in the cavity) and transmitted field (in the transmission line). We prepare an input state in the cavity and then release half of its energy while recording the output field. This ‘half-release’ corresponds to a 50:50 beam splitter, for which we expect maximally entangled states. After switching off the conversion process, we immediately perform a single-shot, high-fidelity ($\gtrsim 0.95$) measurement on the cavity. The non-classical correlations between recorded field and cavity outcomes measured in different bases are indicative of the generation of entanglement (Fig. 4a). We demonstrate this using two different state encodings, single photons and cat states.

Half-releasing the Fock state $|1\rangle$ results in the Bell-state $(|1\rangle|0\rangle + |0\rangle|1\rangle)/\sqrt{2}$, where the first ket is the state inside the cavity, and the second the travelling state. When we measure the cavity in the number basis and find it to be in the state $|0\rangle$ ($|1\rangle$), we expect to find the travelling state in $|1\rangle$ ($|0\rangle$). This is revealed with near-ideal contrast in the Q-functions from the travelling field, conditioned on cavity outcomes (Fig. 4b, left column). To show non-classicality in the correlations, we measure the cavity also in a rotated basis to probe the states $(|0\rangle \pm |1\rangle)/\sqrt{2}$. Conditioning on

the outcomes, we find that the Q-functions closely resemble those of $(|0\rangle \pm |1\rangle)/\sqrt{2}$, consistent with a high-fidelity entangled state. This data allows us to further confirm the presence of entanglement through a simple witness. We estimate a lower bound on fidelity compared with the ideal Bell-state of 0.91 ± 0.02 ; this clearly exceeds the classical bound of 0.5 and confirms that the half-release generates entanglement (Supplementary Information).

Although entanglement with single travelling photons can also be observed with two-level systems²⁰, the conversion method presented here can generate entanglement between non-classical multiphoton states. In particular, half-release of a cat state $|C_{\sqrt{2}}^{\pm}\rangle$ generates the entangled state $|\alpha\rangle|\alpha\rangle + |-\alpha\rangle|-\alpha\rangle = |C_{\alpha}^{\pm}\rangle|C_{\alpha}^{\pm}\rangle + |C_{\alpha}^{-}\rangle|C_{\alpha}^{-}\rangle$, where we have omitted normalization factors. Although such two-mode entangled cat states have been created previously in locally coupled oscillators²⁹ and with itinerant optical photons³⁴, our scheme realizes an interface between stationary and flying cats. We demonstrate this ‘Schrödinger catapult’ by half-releasing the cat state $|C_{\sqrt{2}}^{\pm}\rangle$. To show non-classical correlations we measure the cavity in the coherent-state basis, finding it in either $|\pm\alpha\rangle$, or in the parity basis, thus finding it in either the even or odd cat state $|C_1^{\pm}\rangle$. The conditioned Q-functions of the flying field are shown in Fig. 4c. Again, the correlations are consistent with a high-fidelity entangled state. A slight reduction of contrast in the coherent-state basis results

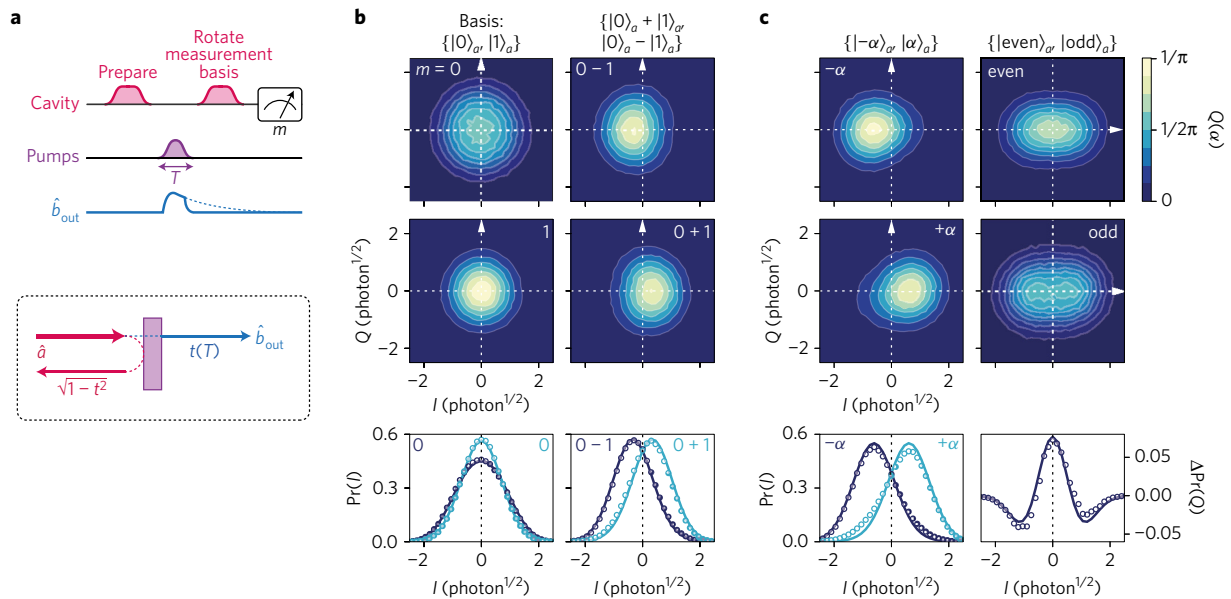


Figure 4 | Generating entanglement between stationary and travelling fields. a, We partially release the cavity field by applying the pumps for a reduced amount of time. We condition the recorded field on the outcome of a subsequent measurement of the cavity to obtain correlations. Partial release is analogous to a field impinging on a partially transmitting mirror, where the transmittance t is set by the pump time T . **b**, Half-release of $|1\rangle$. Left column: Q -functions conditioned on finding the cavity in either $|0\rangle$ or $|1\rangle$. Right column: finding the cavity in either $|0\rangle + |1\rangle$ or $|0\rangle - |1\rangle$. Lower panels: Marginals, obtained by integration along Q . **c**, Half-release of $|C^+_{\sqrt{2}}\rangle$. Left: conditioned on finding the cavity in either $|-\alpha\rangle$ or $|+\alpha\rangle$. Right: conditioned on finding either an even or odd number of photons in the cavity. Lower left: Marginals, obtained by integration along I . Lower right: for the parity-conditioned data we show the difference in the marginals. Solid lines: ideal case (perfect entangled state and perfect cavity measurement), taking into account only the detection efficiency in the Q -functions. All data have been taken with $g/2\pi = 164$ kHz and 10^6 samples per state and basis.

from state evolution due to the Kerr effect, which reduces the fidelity of the cavity measurement (Supplementary Information).

This entanglement between stationary and travelling cats will enable error-correctable distribution of entanglement. Capture of the wave packet emitted by half-release enables the creation of remote entanglement between stationary parties. For the cat states used in this work, any photon loss in the transmission channel will corrupt the state because it results in change of parity. However, photon loss becomes detectable when we half-release a cat state of the form $|\alpha\rangle + |\alpha\rangle + |-\alpha\rangle + |-\alpha\rangle$ (ref. 35). Such states are eigenstates of ‘superparity’ with modulo 4 photons, and even/odd (modulo 2) parity measurements can be used to detect and correct single-photon loss¹⁷. Thus, measuring and comparing the parity between the remote parties will allow for detection and correction of single-photon loss in the transmission line during remote entanglement generation.

Summary and outlook

We have shown the coherent release of quantum states from a microwave cavity memory. This release is enabled by parametric upconversion utilizing the nonlinearity of a single Josephson junction. This conversion scheme fulfils our requirements for an interface between stationary and travelling oscillator states in a microwave quantum network: we can dynamically control the conversion rate, releasing cavity states almost 1,000 times faster than the intrinsic lifetime. This conversion rate is state-independent for states containing up to a few photons, extendable to up to tens by simple hardware adjustments (Supplementary Information). The release process is equivalent to a beam splitter interaction, and cavity states are mapped faithfully onto travelling states. This interaction can be controlled precisely and rapidly, enabling the generation of entanglement between cavity and travelling modes.

Our interface can serve as the backbone in a microwave quantum network in which quantum information is stored in cavities. Since the conversion process is controllable in amplitude and phase, it

will allow quantum state transfer and entanglement between remote cavities¹⁸ (Supplementary Information). The scheme presented supports multidimensional Hilbert spaces, thus providing a route towards error-correctable distribution of quantum information and entanglement. The on-demand generation of arbitrary, travelling multiphoton quantum states shown provides further exciting new opportunities for hybrid quantum systems. For instance, the efficient capture of travelling microwave fields by mechanical oscillators has been demonstrated experimentally³⁶. Our ‘catapult’ can therefore be used to create highly non-classical mechanical states. Mechanical systems can act as transducers with radically different degrees of freedom, such as light in the optical domain^{37,38}. The combination of our system with such a transducer will thus enable the distribution of exotic continuous variable quantum states in heterogeneous networks.

Data availability. The data that support the plots within this paper and other findings of this study are available from the corresponding author upon reasonable request.

Received 15 December 2016; accepted 18 April 2017;
published online 5 June 2017

References

- Kimble, H. J. The quantum internet. *Nature* **453**, 1023–1030 (2008).
- Nickerson, N. H., Li, Y. & Benjamin, S. C. Topological quantum computing with a very noisy network and local error rates approaching one percent. *Nat. Commun.* **4**, 1756 (2013).
- Ritter, S. *et al.* An elementary quantum network of single atoms in optical cavities. *Nature* **484**, 195–200 (2012).
- Monroe, C. *et al.* Large-scale modular quantum-computer architecture with atomic memory and photonic interconnects. *Phys. Rev. A* **89**, 1–16 (2014).
- Bernien, H. *et al.* Heralded entanglement between solid-state qubits separated by three metres. *Nature* **497**, 86–90 (2013).
- Gottesman, D., Kitaev, A. & Preskill, J. Encoding a qubit in an oscillator. *Phys. Rev. A* **64**, 012310 (2001).

7. Monroe, C., Meekhof, D. M., King, B. E. & Wineland, D. J. A “Schrodinger Cat” superposition state of an atom. *Science* **272**, 1131–1136 (1996).
8. Signoles, A. *et al.* Confined quantum Zeno dynamics of a watched atomic arrow. *Nat. Phys.* **10**, 715–719 (2014).
9. McConnell, R., Zhang, H., Hu, J., Čuk, S. & Vuletić, V. Entanglement with negative Wigner function of almost 3,000 atoms heralded by one photon. *Nature* **519**, 439–442 (2015).
10. Ourjoumtsev, A., Tualle-Brouiri, R., Laurat, J. & Grangier, P. Generating optical Schrödinger kittens for quantum information processing. *Science* **312**, 83–86 (2006).
11. Neergaard-Nielsen, J. S., Nielsen, B. M., Hettich, C., Mølmer, K. & Polzik, E. S. Generation of a superposition of odd photon number states for quantum information networks. *Phys. Rev. Lett.* **97**, 083604 (2006).
12. Deléglise, S. *et al.* Reconstruction of non-classical cavity field states with snapshots of their decoherence. *Nature* **455**, 510–514 (2008).
13. Hofheinz, M. *et al.* Synthesizing arbitrary quantum states in a superconducting resonator. *Nature* **459**, 546–549 (2009).
14. Kirchmair, G. *et al.* Observation of quantum state collapse and revival due to the single-photon Kerr effect. *Nature* **495**, 205–209 (2013).
15. Bretheau, L., Campagne-Ibarcq, P., Flurin, E., Mallet, F. & Huard, B. Quantum dynamics of an electromagnetic mode that cannot contain N photons. *Science* **348**, 776–779 (2015).
16. Reagor, M. *et al.* Quantum memory with millisecond coherence in circuit QED. *Phys. Rev. B* **94**, 014506 (2016).
17. Ofek, N. *et al.* Extending the lifetime of a quantum bit with error correction in superconducting circuits. *Nature* **536**, 441–445 (2016).
18. Cirac, J. I., Zoller, P., Kimble, H. J. & Mabuchi, H. Quantum state transfer and entanglement distribution among distant nodes in a quantum network. *Phys. Rev. Lett.* **78**, 3221–3224 (1997).
19. Houck, A. A. *et al.* Generating single microwave photons in a circuit. *Nature* **449**, 328–331 (2007).
20. Eichler, C., Bozyigit, D. & Wallraff, A. Characterizing quantum microwave radiation and its entanglement with superconducting qubits using linear detectors. *Phys. Rev. A* **86**, 032106 (2012).
21. Srinivasan, S. J. *et al.* Time-reversal symmetrization of spontaneous emission for quantum state transfer. *Phys. Rev. A* **89**, 033857 (2014).
22. Pechal, M. *et al.* Microwave-controlled generation of shaped single photons in circuit quantum electrodynamics. *Phys. Rev. X* **4**, 1–9 (2014).
23. Yin, Y. *et al.* Catch and release of microwave photon states. *Phys. Rev. Lett.* **110**, 107001 (2013).
24. Pierre, M., Svensson, I.-M., Raman Sathyamoorthy, S., Johansson, G. & Delsing, P. Storage and on-demand release of microwaves using superconducting resonators with tunable coupling. *Appl. Phys. Lett.* **104**, 232604 (2014).
25. Flurin, E., Roch, N., Pillet, J. D., Mallet, F. & Huard, B. Superconducting quantum node for entanglement and storage of microwave radiation. *Phys. Rev. Lett.* **114**, 090503 (2015).
26. Schuster, D. I. *et al.* Resolving photon number states in a superconducting circuit. *Nature* **445**, 515–518 (2007).
27. Heeres, R. W. *et al.* Implementing a universal gate set on a logical qubit encoded in an oscillator. Preprint at <http://arXiv.org/abs/1608.02430> (2016).
28. Nigg, S. E. *et al.* Black-box superconducting circuit quantization. *Phys. Rev. Lett.* **108**, 240502 (2012).
29. Wang, C. *et al.* A Schrodinger cat living in two boxes. *Science* **352**, 1087–1091 (2016).
30. Bergeal, N. *et al.* Phase-preserving amplification near the quantum limit with a Josephson ring modulator. *Nature* **465**, 64–68 (2010).
31. Leonhardt, U. *Measuring the Quantum State of Light* (Cambridge Univ. Press, 1997).
32. Bertet, P. *et al.* Direct measurement of the Wigner function of a one-photon Fock state in a cavity. *Phys. Rev. Lett.* **89**, 200402 (2002).
33. Michael, M. H. *et al.* New class of quantum error-correcting codes for a bosonic mode. *Phys. Rev. X* **6**, 031006 (2016).
34. Ourjoumtsev, A., Ferreyrol, F., Tualle-Brouiri, R. & Grangier, P. Preparation of non-local superpositions of quasi-classical light states. *Nat. Phys.* **5**, 189–192 (2009).
35. Roy, A., Stone, A. D. & Jiang, L. Concurrent remote entanglement with quantum error correction against photon losses. *Phys. Rev. A* **94**, 032333 (2016).
36. Andrews, R. W., Reed, A. P., Cicak, K., Teufel, J. D. & Lehnert, K. W. Quantum-enabled temporal and spectral mode conversion of microwave signals. *Nat. Commun.* **6**, 10021 (2015).
37. Bochmann, J., Vainsencher, A., Awschalom, D. D. & Cleland, A. N. Nanomechanical coupling between microwave and optical photons. *Nat. Phys.* **9**, 712–716 (2013).
38. Andrews, R. W. *et al.* Bidirectional and efficient conversion between microwave and optical light. *Nat. Phys.* **10**, 321–326 (2014).

Acknowledgements

We thank J. Blumoff, K. Chou, M. Constantin and M. Reagor for experimental assistance, and K. Sliwa and A. Narla for help setting up the parametric amplifier. We gratefully acknowledge valuable discussions with S. M. Girvin, R. Hanson, Z. Leghtas, K. W. Lehnert, A. Narla, A. Reed, S. Shankar and S. Touzard. This research was supported by the US Army Research Office (W911NF-14-1-0011). W.P. was supported by NSF grant PHY1309996 and by a fellowship instituted with a Max Planck Research Award from the Alexander von Humboldt Foundation; W.P. and P.R. by the US Air Force Office of Scientific Research (FA9550-15-1-0015); C.J.A. by an NSF Graduate Research Fellowship (DGE-1122492); L.D.B. by the ARO QuaCGR Fellowship; L.J. by the Alfred P. Sloan Foundation and the Packard Foundation. Facilities use was supported by the Yale Institute for Nanoscience and Quantum Engineering (YINQE), the Yale SEAS cleanroom, and the National Science Foundation (MRSECDMR-1119826).

Author contributions

W.P., C.J.A. and L.D.B. took and analysed the data, and performed theoretical modelling with input from U.V.; C.J.A. fabricated the device; P.R. contributed to the measurement software; W.P., C.J.A., L.D.B. and R.J.S. wrote the manuscript with input from all authors. R.J.S. supervised the project.

Additional information

Supplementary information is available in the [online version of the paper](#). Reprints and permissions information is available online at www.nature.com/reprints. Publisher's note: Springer Nature remains neutral with regard to jurisdictional claims in published maps and institutional affiliations. Correspondence and requests for materials should be addressed to W.P.

Competing financial interests

R.J.S., M.H.D. and L.F. are founders and equity shareholders of Quantum Circuits, Inc.